ATTENUATION OF DROPLET IMPACTS ON TI ALLOY CAUSED BY SUBMERGED CONDITIONS

JAKUB POLOPRUDSKY[1*], GABRIEL STOLARIK[2], ALICE CHLUPOVA[1]

[1] Institute of Physics of Materials, The Czech Academy of Sciences, Brno, Czech Republic

[2] Faculty of Manufacturing Technologies TUKE with a seat in Presov, Slovak Republic

DOI: 10.17973/MMSJ.2025_06_2025053

Corresponding author: poloprudsky@ipm.cz

The research focuses on cyclic collisions of water droplets with a solid surface of titanium alloy Ti6Al7Nb in varying environments between the nozzle and the impacted surface. The source of repeated impacts is an ultrasonically driven pulsating water jet. Each experimental run consisted of repeated droplet impacts at a starting frequency of 20 kHz concentrated on a single point with variance in exposure time from 1 to 10 s with 0.5 s increment. Two environments were used as the medium between the nozzle and the impacted surface, i.e., air and water. Differences in erosion effect under atmospheric and submerged conditions were followed regarding maximum erosion depth and removed volume. The droplet attenuation due to interference of the water jet with the water environment had detrimental effects on the maximum erosion depth achieved, reaching only 10 to 6 % compared to atmospheric conditions. A similar situation has been observed in the case of volume removed.

KEYWORDS

pulsating water jet, water cluster, droplet, erosion, submerged, impact attenuation, atmospheric drag

1 INTRODUCTION

Cyclic loading of surface by repetitive liquid impact pressure attained using an ultrasonic pulsating water jet (PWJ) in atmospheric conditions has attracted lot of attention. Erosion of metals due to repeated impingement generally evolves in three stages of erosion based on the exposure time [Thomas 1970, Foldyna 2012]. The first stage, often called incubation, is related to short exposure to water jetting. It precedes macroscopical material removal and is characterized by changes in the surface and subsurface of the target material. The second erosion stage is characterized by pit formation and the highest erosion rate, while the third stage shows a lower erosion rate and merging of erosion pits. Some authors further divide the erosion curve into five stages, including incubation, acceleration, maximum rate, deceleration, and terminal stage [Ma 2015, Elhadi Ibrahim 2020]. This division helps to describe the transition regions between the stages better.

Several studies have shown that the distance between the nozzle and the treated surface, known as standoff distance (SOD), has a significant effect on water droplet development and the resulting erosion [Lehocka, 2019; Srivastava, 2020; Nag, 2024; Poloprudský, 2019]. In the case of a short standoff distance, the jet acts continuously as the velocity waves caused by sonotrode oscillations do not have enough space to separate the jet into individual droplets. At more considerable distances, the velocity fluctuations cause the separation of the jet into discrete water droplets, and the erosion potential of the jet increases due to impact pressure. Another increase in standoff distance nevertheless results in a decrease in PWJ efficiency due to atmospheric drag and severe decohesion of the jet. To obtain the highest PWJ efficiency, the adjustment of at least two parameters is necessary, i.e., the optimum length of the acoustic chamber of sonotrode [Nag 2019] and the optimum stand-off distance [Hloch 2020].

The situation with the decomposition of water jet due to atmospheric drag in the air environment also applies to different mediums, such as water. Several studies already focused on water jetting in submerged conditions [Ben-Mansour 2021; Haghbin 2015; Hloch 2024; Stolárik 2024; Wright 2013; Yadav 2016].

The studies of the degradation effect of erosion in submerged conditions play an important role in the case of damage to hydraulic systems and parts such as pipe bends [Ben-Mansour 2021]. In many applications, atmospheric conditions are not attained, and the jet has to be used while submerged in a liquid medium, for example, in the case of cleaning structures located below the water surface. The advantages of a high-pressure water jet are the ability to use local water for cleaning and the simultaneous collection of removed biofoulings [Song 2020, Albitar 2016]. Another application, when a waterjet acts in a different environment than air, is in the human body in the case of special orthopedic operations [den Dunnen 2013]. Submerged conditions can be successfully exploited, providing beneficial results. For example, reduced kerf taper and improved surface finish were observed in submerged conditions compared to atmospheric conditions when using an abrasive water jet [Haghbin 2015]. This technique seems highly promising in submerged cutting in offshore applications [Louis 2007].

Compared to continuous water jets at the same hydraulic conditions, the pulsating water jet technique has higher erosion effectiveness, as confirmed in [Nag 2023], where water jetting was used for piercing ductile materials. However, a very limited number of studies were done concerning the erosion effectivity of PWJ in submerged conditions [Hloch 2024, Stolárik 2024, Szada-Borzyszkowska 2023, Yadav 2016]. The drag effect of the liquid environment dampening the hammering effect of liquid droplets impinging on the surface has to be considered, along with the possible effect of cavitations on the eroded surfaces due to submerged jet cavitation potential [Wright 2013].

The research in this work focuses on the cyclic collisions of water droplets created by the pulsating water jet technique with a solid surface in two environments, i.e., air and water, when the water level for submerged conditions was 150 mm. The material under investigation is titanium alloy Ti6Al7Nb, widely used in biomedical applications.

Based on previous experiments of successful surface modification [Stolárik 2024], a pressure of 70 MPa and a nozzle diameter of 0.8 mm were chosen. The results of the previous study demonstrated a significant difference in atmospheric and submerged conditions on erosion and therefore a deeper analysis of the course of erosion stages within the given PWJ settings is necessary. Especially considering complex movement pattern of the jet in previous study [Stolárik 2024], current study dwells into underlying material removal mechanisms by employing stationary PWJ jet creating erosion damage in localized area. The target Ti6Al7Nb sample was loaded for a time range of 1 – 10 s with an increment of 0.5 s, which

provided a sufficient load range to monitor the erosion development in all erosion stages.

2 MATERIAL AND METHODS

2.1 Material

Titanium alloy Ti6Al7Nb is widely used in biomedical applications. It has similar mechanical and metallurgical properties as Ti6Al4V, but vanadium was replaced by niobium to increase biocompatibility, as some researchers suspect the negative influence of vanadium [Siemers 2018]. Chemical distribution is shown in Fig.1, hinting phases distribution as Nb stabilizes β-phase while Al stabilizes α-phase The material was received in the form of a rolled sheet with hardness evaluated from 5 measurement as 334±7HV1

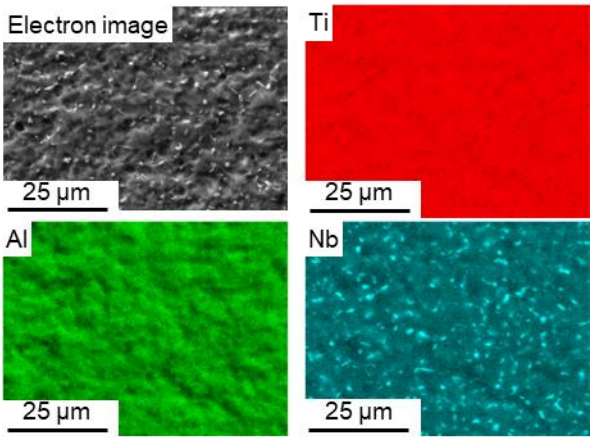

Figure 1 EDS analysis of Ti6Al7Nb surface before PWJ experiment.

2.2 Experiment

During the experiment, the rolled surface of Ti6Al7Nb was exposed to repeated droplet impingement under atmospheric and submerged conditions with a water level of 150 mm (see the scheme in Fig. 2).

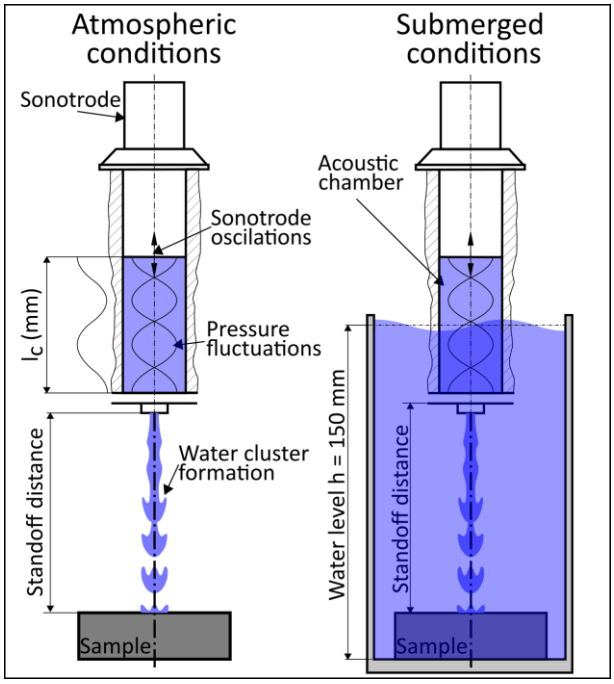

Figure 2 Schematic of the pulsating water jet with an acoustic generator causing pressure fluctuations and adjustable acoustic chamber under atmospherics and submerged conditions with 150 mm water level.

The PWJ head as a droplet generator was positioned stationary above the flat surface of the treated material, so the individual erosion craters in the form of "dots" were created. Each combination of experimental conditions was repeated three times to increase the statistical significance of the experiment. The photo documentation from the experiment and the samples created are shown in Fig.3.

Setting	Run No.	p	f	Flow speed	Optimal standoff	Exp. time	Interval	No of impacts
-	-	*MPa*	*kHz*	*m/s*	*mm*	*s*	*s*	-
Atmospheric	1	70	19.39	337	43	1-10	0.5	19 390-193 900
Atmospheric	2	70	19.38	337	43	1-10	0.5	19 380-193 800
Atmospheric	3	70	19.38	337	43	1-10	0.5	19 380-193 800
Submerged	1	70	19.57	337	46	1-10	0.5	19 570-195 700
Submerged	2	70	19.57	337	46	1-10	0.5	19 570-195 700
Submerged	3	70	19.57	337	46	1-10	0.5	19 570-195 700

Table 1 Technological parameters of PWJ experiment.

The supply hydraulic pressure in the acoustic chamber of the sonotrode was set to 70 MPa to reach a flow speed of 337 m/s, considering a discharge coefficient of 0.9. The nozzle diameter selected for the experiment was 0.8 mm. Therefore, a flow rate of 0.000169 m^3/s (10.17 l/min) was achieved. The exposure time of the treated area was increased from 1 s to 10 s with an increment of 0.5 s using 20 kHz sonotrode. The actual working frequency read during the experiment is listed in Tab. 1, together with other technological parameters used. A combination of frequency and exposure time gives the number of impacts in the range, which roughly equates to a value between 20,000 and 200,000 impacts. Optimal standoff distance was evaluated independently for each medium using stair trajectory as described by Hloch [Hloch 2020]. According to Nag, the optimal length of the acoustic chamber was also evaluated independently for atmospheric and submerged conditions [Nag 2019].

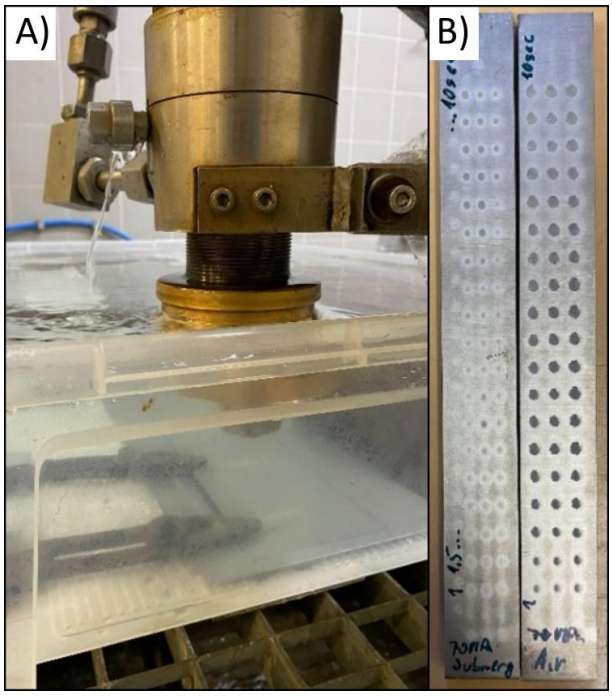

Figure 3 a) Photo of experimental set-up for submerged conditions and b) samples with erosion craters for submerged (left) and atmospheric conditions (right).

2.3 *Measurement*

The InfiniteFocus G5focus variation-based non-contact optical 3D measurement system was used to quantitatively assess erosion in terms of maximum depth, mean depth, and volumetric mass removal. The depth values of erosion craters achieved by PWJ treatment were evaluated from the surface profile and the calculated values of the removed volume. Each value was averaged from three measured erosion craters.

Tescan LYRA 3 XMH FEG/SEM scanning electron microscope with FEG electron source was employed to evaluate the presence and type of erosion features. Primary observation was conducted using a secondary electron detector to enhance edges and surface features. Additional observations were carried out using a backscattered electron detector to enhance chemical contrast in the material and highlight material phases.

3 RESULTS AND DISCUSSION

Fig. 4 shows the effect of the environment (air and water) on the erosion by PWJ of Ti alloy as plots of dependences of maximum depth, mean depth, and volume of material removed by erosion on exposure time. All three measured parameters show an increasing tendency with increased exposure time. The equations of the fits are added to the graphs (Fig. 4), green for atmospheric conditions and blue for submerged conditions.

In the case of atmospheric conditions, the increase in depths (max., mean) and volume removed is apparent since the lowest exposure time is 1 s from the range in this experiment. It means that the material enters the acceleration erosion stage, according to [Elhadi Ibrahim 2020], or the second erosion stage, according to [Thomas 1970]. Exposure longer than 1 s leads to a rapid increase in measured values of depth and volume removed. The maximum erosion rate lasts for approximately five s. Further increase in exposure time slows down erosion efficiency.

It signifies entering the deceleration or terminal stage of erosion. The max depth increases from 12.2 µm for 1 s to 277.6 µm for 10 s exposure.

In the case of atmospheric conditions, it is possible to observe larger deviations of the measured values for the monitored parameters (depth, volume) compared to submerged conditions. In the case of a time interval of up to 3 s, the material may be surface damaged in the form of cracks and macroscopic removal of material from the surface. However, after 3 s, localized removal of material occurs, which also causes a higher measured scatter of values. This shows that atmospheric conditions erode the target material non-uniformly. Erosion may be accompanied by peeling of larger fragments of the target material, which also leads to larger irregularities on the bottom of the crater. In the case of submerged conditions, this was reduced by the reduction of the impact pressure of the water droplets due to resistance of surrounding water. The water droplets in the water medium come into contact with the surrounding static water immediately after exiting the nozzle. This means that their energy is also consumed to drive the surrounding static water. This effect is most significant on the outer parts of the water droplets that interact and propel the static water. Therefore, submerged conditions not only cause a reduction in the energy of the water droplets, but also a radial reduction in their size. This will be reflected in the reduction of the erosion potential. The propulsion of the surrounding static water will also be reflected in the formation of turbulent regions, which also contributes to the reduction of the axial velocity of the water stream [Xiaohui 2021]. In a study [Xiaohui 2021] showed that after exceeding a critical distance from the nozzle, there is a radical reduction in the axial velocity of the water stream.

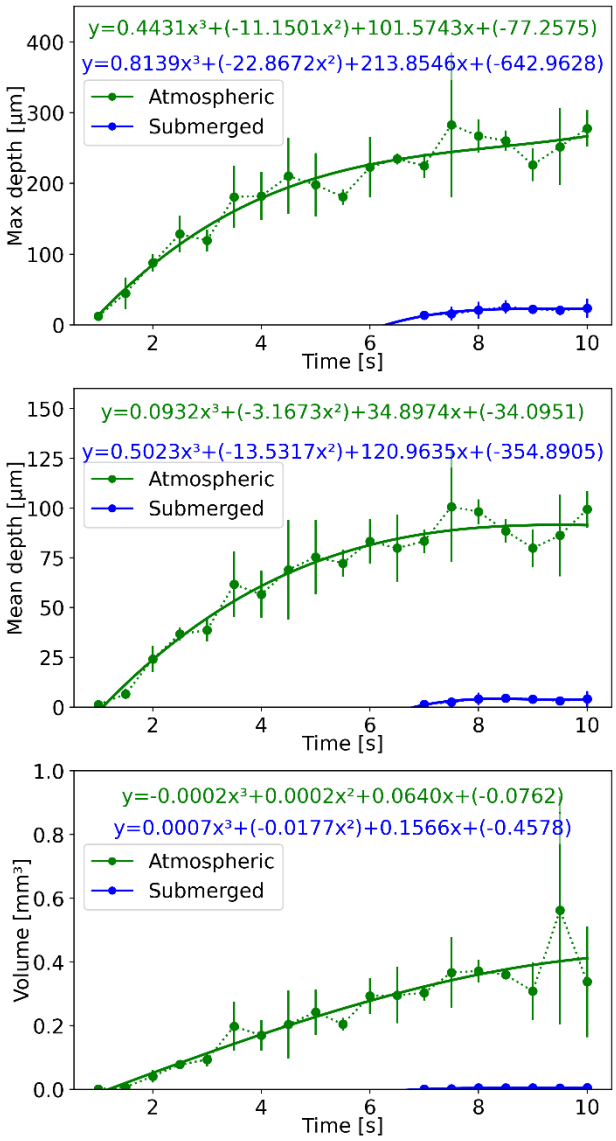

Figure 4 Dependences of maximum depth, mean depth, and removed volume on increasing exposure time for atmospheric (green) and submerged (blue) conditions.

Contrary to the air environment, in the case of submerged conditions, the first measurable depths (max, mean) and volume removed were obtained for 7 s of exposure. The max depth observed after 7 s of exposure, i.e., at the beginning of the acceleration stage of erosion, reaches a value of 13.7 µm. The value obtained in submerged conditions after 7 s is similar to that obtained under atmospheric conditions after only 1 s of exposure (12.16 µm), therefore onset of erosion acceleration stage was delayed by 6s in case of submerged jet exposure. The max depth increases gradually to 23.7 µm for 10 s exposure in submerged conditions, which is, only 8.5 % of max depth reached by atmospheric conditions (277.6 µm).

This confirms the theory of the reduction of the energy of the water droplets consumed to propel the surrounding static water. The drag caused by static water can lead to lowering the speed of water droplet impingement leading to lower impact pressure below material erosion resistance threshold for given number of impingements. It is also necessary to say that in submerged conditions this erosion development was observed when the stand-off distance was increased from 43 mm in air to 46 mm in submerged conditions. This increase could be

attributed to the phenomenon of "tunneling" when the water droplets have to break through the static water. Constant propulsion of the surrounding water in the direction of the flow can lead to the surrounding water theoretically increasing the volume of the droplets, which will be reflected in the change in optimal stand-off distance.

In the case of data concerning the eroded volume, the decrease in erosion efficiency in submerged conditions is even more substantial. The volume removed for atmospheric conditions starts at 1 s exposure with the value of 0.0005 mm^3 and goes to 0.3376 mm^3 for 10 s. The removed volume under submerged conditions increased from 0.0004 mm^3 for exposure of 7 s to 0.0050 mm^3 for exposure of 10 s. Considering exposure of 10 s, submerged conditions (0.0050 mm^3) reached only 1.5 % of volume removed by atmospheric conditions (0.337596 mm^3), showing decrease in erosion efficiency due to interaction between water droplets created by the PWJ and stationary water in the jet trajectory.

Tab. 2 shows the maximum depth and volume removed assessed for the exposure time range from 7 s to 10 s for both conditions. The third column shows the % attenuation caused by the water column between the nozzle and the sample in submerged conditions. Calculation of this parameter considers the atmospheric value as 100 % and, based on it, calculates submerged % attenuation for submerged conditions. Attenuation in the case of maximum depth reaches a value over 90 %. In the case of removed volume, attenuation is even more severe, reaching values of over 98.5 % in the interval under investigation.

The level of attenuation considering a water level of h = 150 mm in our work is in strong contrast to a similar study concerning droplet erosion under stationary PWJ of aluminum alloy and copper done by Hloch [Hloch 2024]. Their experiments compared atmospheric and submerged conditions with two water levels of 80 and 120 mm. When we use the values of erosion depth analogically to our work for recalculation of attenuation, we obtain the following drag effect of the water column on a jet in the case of Al-alloy. For 1 s exposure, the attenuation reaches values of 7 and 24 % for water level h of 80 and 120 mm. 2 s exposure led to relative attenuation of 15 % and 25 % for h = 80 mm and 120 mm, respectively.

A massive difference in attenuation between our experiments and results published in [Hloch 2024] cannot be wholly attributed to increased water level. However, it is assumed that it is related also to material properties.

In our study, due to water resistance, droplet speed was reduced to a level where impact pressure is near or below characteristic material properties, which defines material resistance to repeated impact (hardness, yield strength, fatigue strength, etc.).

Exp. time	Max depth			Removed volume		
-	*Atmo.*	*Subm.*	***Atten.***	*Atmo.*	*Subm.*	***Atten.***
[s]	*[µm]*	*[µm]*	***[%]***	*[mm^3]*	*[mm^3]*	***[%]***
7	224.8	13.7	**93.9**	0.302638	0.0004	**99.9**
7.5	282.7	15.8	**94.4**	0.366509	0.0014	**99.6**
8	267.1	20.9	**92.2**	0.371178	0.0041	**98.9**
8.5	260.1	25.4	**90.2**	0.359314	0.0045	**98.8**
9	226.1	22.3	**90.1**	0.307751	0.0039	**98.7**
9.5	251.7	20.7	**91.8**	0.562255	0.0032	**99.4**
10	277.6	23.7	**91.5**	0.337596	0.0050	**98.5**

Table 2 Maximum depth achieved and removed volume for atmospheric (air) and submerged conditions and the respective percentual attenuation of submerged conditions.

Fig. 5 presents the results of observation of erosion craters by SEM. The SEM micrographs show the overview taken at magnification 50x of selected erosion craters. The first signs of macroscopic material removal under atmospheric conditions were visible after 2 s exposure. Compared to that, for submerged conditions, a similar appearance of macroscopic material removal starts to be visible for 8 s exposure. This is in good agreement with the results of depth and volume measurement (see Fig.4). However, it is necessary to point out that 8 s exposure is related to the beginning of the acceleration stage of erosion, while the preceding incubation phase, which is typical with surface roughening and tiny changes in surface and subsurface of material already occurred. This stage is challenging to capture by low magnification SEM, and results are highly subjected to brightness and contrast settings, which lead to similar appearance of 8 s and 10 s at this magnification level. This similarity between 8 and 10s can be also explained by saturating the character of erosion curves at this exposure time (Fig. 4).

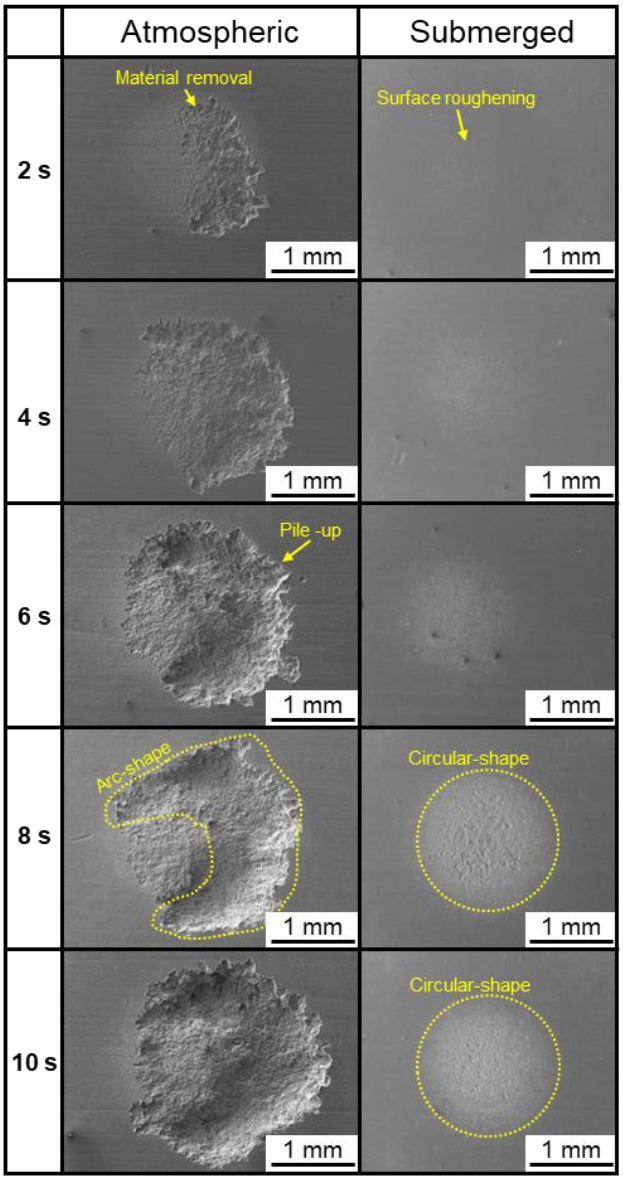

Figure 5 Comparison of SEM micrograph with an overview of erosion craters created in atmospheric and submerged conditions based on exposure time.

Another important fact detected from the images in Fig. 5 is a difference in the shapes of the erosion marks for atmospheric and submerged conditions. Generally, the stationary jetting of the surface of the material results in the creation of erosion craters in the form of dots. Nevertheless, under atmospheric conditions, the PWJ exposure creates preferentially craters exhibiting arc-shape patterns, as seen by many other studies [Poloprudsky 2021, Poloprudsky 2024, Hloch 2024 b]. This inhomogeneity can be related to inhomogeneous flow fields in the nozzle [Hong 2023]. The asymmetry in the erosion effect can also be observed in the case of jetting with traverse speed when, instead of one erosion crater in the form of the dot, a linear erosion groove is formed. In that case, the asymmetry can be observed as different borders of erosion groove on one and opposite sides, as reported in [Hloch 2022]. On the other hand, droplet impact in submerged conditions creates an erosion crater with a circular pattern. Similarly, Haghbin et al. [Haghbin 2015] observed improved kerf taper in submerged conditions, possibly attributed to flow stabilization. This could be beneficial for applications where a highly predictable and repeatable shape/topography/morphology is desired, including surface treatment [Stolárik 2024] or cleaning [Albitar 2016].

Fig. 6 presents higher magnification (500x) SEM micrographs of the central region of each crater for selected exposures. Similarly, as in the case of Fig. 5, appearance and typical signs are compared for atmospheric and submerged conditions.

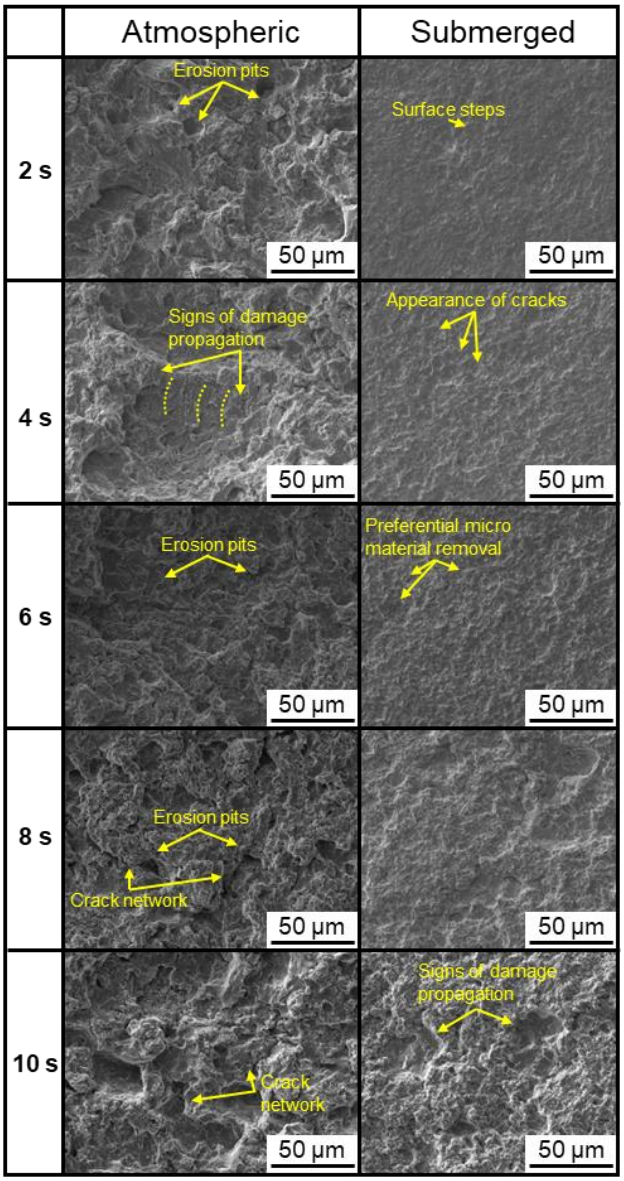

Figure 6 SEM overview comparison of erosion craters created in atmospheric and submerged conditions based on exposure time.

Under atmospheric conditions, typical features present on the PWJ-treated surface of the material include erosion pits caused by direct water droplet impact and following signs of hydraulic penetration into created cracks. The surface is very serrated, with many high peaks and deep valleys. Occasional occurrence of smoothened plateaus was observed. The surface shows a high number of cracks in different stages of development. There are short singular cracks, cracks encircling surface parts, and interconnected crack networks visible from the surface. Similar features were reported in [Poloprudsky 2022, Nag 2023, Hloch 2024 b]. Contrary to the work of Hloch concerning the CT-based study on aluminum [Hloch 2022], suggesting that cracks and tunnels may be further interconnected below the surface. Similar tunneling mechanism was described also by [Stolárik 2023]. The expressive creation of subsurface tunnels was not observed in our case. The detail of the 4 s exposure under atmospheric conditions shows the presence of arranged lines/curves related to the action of lateral jetting in the bottom of the erosion crater. These lines may hint at local damage initiation and the direction of damage propagation,

and, therefore, they strongly resemble the fatigue damage propagation signs known as striations. This can be considered as proof that PWJ damage is (at least partially) cyclical in nature.

For submerged conditions, the erosion starts as surface roughening (2 s) and continues with further exposure in this incubation erosion stage. 4 s exposure leads to the first appearance of visible cracks. As these cracks propagate, material removal starts at the microscopic level (6 s). Further exposure leads to crack propagation and increases the size of areas with removed material. After 10 s exposure in submerged conditions, the surface shows erosion features similar to those under atmospheric conditions for 2 s exposure.

The highest magnification of 5,000 x was used in SEM observation to focus on erosion details in the center of the erosion crater, and the comparison of results for both atmospheric and submerged conditions is presented in Fig. 7.

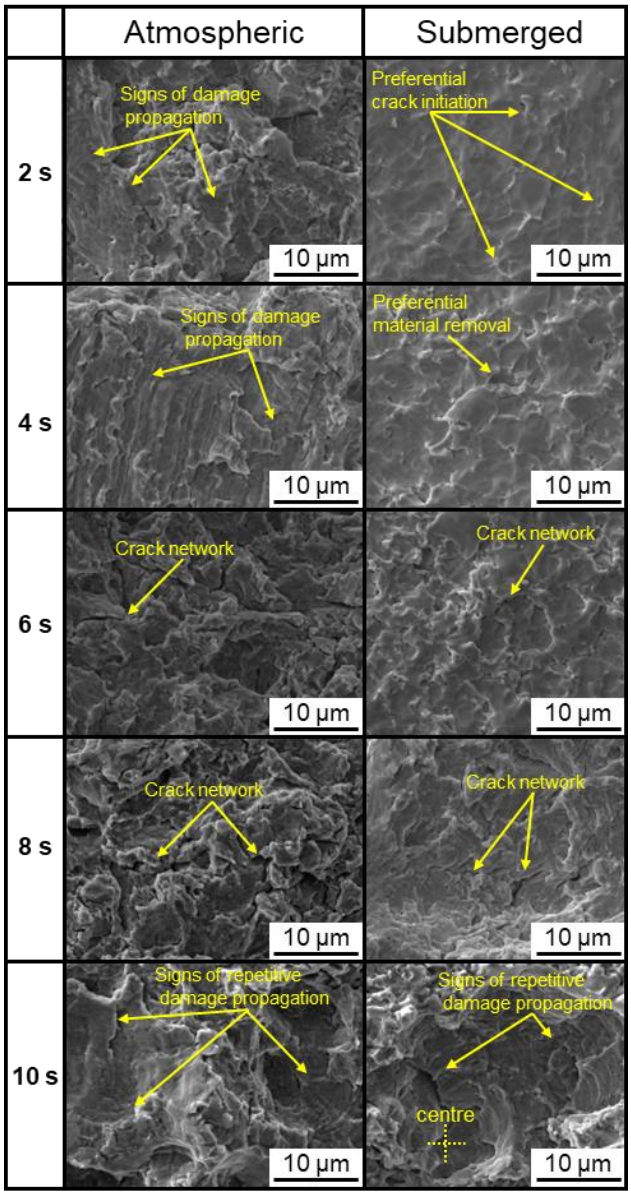

Figure 7 SEM overview comparison of erosion craters created in atmospheric and submerged conditions based on exposure time.

Exposure to droplets in atmospheric conditions exhibits a fractured surface after material removal. After exposure to 2, 4, and 10 s to the action of PWJ, these details show signs of cyclic damage propagation, reported in Fig. 6. These arranged lines/curves show that damage increases periodically. It also indicates the direction of damage propagation. A very similar pattern as was already observed in the case of atmospheric conditions for the lowest exposures was observed in the case of submerged exposure after prolonged exposure of 10 s. In the micrograph for 10 s submerged, the arranged lines/curves are present in several locations, indicating multiple directions of propagation. This can be successfully adopted for assessment of the center of the start of material removal.

2 s exposure in submerged conditions leads to the surface roughening confirmed and by depth/volume measurement (see Fig. 4). However, localized material damage in the form of cracks can be found at this large magnification. The cracks seem to appear on α/β phase interface preferentially. This is also the place where, after further exposure (4 s), material removal starts. This preferential damage is probably caused by the removal of the β phase, which allows for faster water penetration and erosion [Siahpour 2022].

After 6 s and 8 s exposure, interconnected cracks are visible. From the detailed observation of the central part of erosion craters, it can be noted that the surface exposed to submerged droplet impingement shows erosion features similar to those exposed to PWJ under atmospheric conditions. However, the time offset of these features is significantly different.

Fig. 8 shows SE and BSE images of the same place located on the edges of erosion craters created by droplet impingement under atmospheric conditions in the case of 4 s and 6 s exposure. Regarding 4s exposure, the image shows an area with cracks encircling part of the pile-up. This makes this material part susceptible to further damage and removal due to hydraulic penetration and lateral jetting. Details of the edge of the erosion crater created by 6 s of atmospheric exposure show signs of repetitive damage propagation, similar to signs observed at the bottom of the erosion crater.

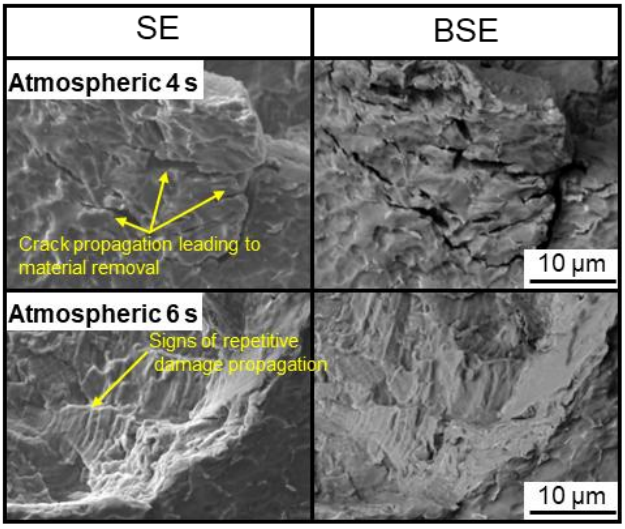

Figure 8 SEM micrographs of features present on the edge of erosion craters. The exact location was captured in SE and BSE modes to relate the present damage features with the phase composition of the sample.

As described in the introduction, the need for submerged applications of water jetting will require (mainly in the case of PWJ) a systematic study of cluster development based on standoff distance in a non-atmospheric environment. This is relevant because optimal working standoff distances of ultrasonically pulsed PWJ devices are significantly higher than in the abrasive water jet in submerged conditions [Haghbin 2015].

4 CONCLUSIONS

This study focused on the attenuation of erosion of Ti alloy caused by pulsating water jet acting under submerged conditions. The following points can state the main findings of this study:

- Submerged conditions lead to strong erosion attenuation of over 90 % in case of maximum depth and over 98.5 % in case of removed volume.

- Signs of repetitive damage propagation have been observed in both atmospheric and submerged conditions.

- Submerged conditions lead to the formation of circular-shaped craters compared to arc-shaped craters created in atmospheric conditions using the same PWJ setting.

- Localized crack initiation and material removal are observed long before macroscopic removal is measured in submerged conditions.

Since the submerged conditions led to significant decrease in pulsating water jet erosion effectivity and there is demand for applications in submerged conditions, this area requires further study. The effect of submerged conditions on structural evolution in reference to atmospheric conditions should be conducted on relevant materials. The proposed method is electron back scattered diffraction analysis. The effect of submerged conditions on PWJ water droplet development and optimal standoff distance should be evaluated. Furthermore, the effect of hydrostatic pressure of surrounding static water on erosion effectiveness should be quantified as it is critical factor in deep water applications.

ACKNOWLEDGMENTS

The financial support by project from The Czech Science Foundation 23-05372S, is gratefully acknowledged. The PWJ treatment was conducted at the Institute of Geonics, The Czech Academy of Sciences.

REFERENCES

[Albitar 2016] Albitar, H., et al. Underwater robotics: surface cleaning technics, adhesion and locomotion systems. International Journal of Advanced Robotic Systems, 2016, Vol.13, No.1. https://doi.org/10.5772/62060

[Ben-Mansour 2021] Ben-Mansour, R., et al. Computational analysis of water-submerged jet erosion. Energies, 2021, *Vol.*14, No.11, 3074. https://doi.org/10.3390/en14113074

[den Dunnen 2013] den Dunnen, S., et al. Waterjet drilling in porcine bone: The effect of the nozzle diameter and bone architecture on the hole dimensions. Journal of the Mechanical Behavior of Biomedical Materials, 2013, Vol.27, pp 84-93. https://doi.org/10.1016/j.jmbbm.2013.06.012

[Elhadi Ibrahim 2020] Elhadi Ibrahim, M., and Medraj M. Water droplet erosion of wind turbine blades: Mechanics, testing, modeling and future perspectives. *Materials,* 2020, Vol.13, No.1, 157. https://doi.org/10.3390/ma13010157

[Foldyna 2012] Foldyna, J., et al. Erosion of metals by pulsating water jet. Tehnicki Vjesnik, 2012, Vol.19, No.2, pp 381-386.

[Haghbin 2015] Haghbin, N., et al. Abrasive waterjet micro-machining of channels in metals: Model to predict high aspect-ratio channel profiles for submerged and unsubmerged machining. Journal of materials processing technology, 2015, Vol. 222, pp 399-409. https://doi.org/10.1016/j.jmatprotec.2015.03.026

[Hloch 2020] Hloch, S., et al. Effect of pressure of pulsating water jet moving along stair trajectory on erosion depth, surface morphology and microhardness. Wear, 2020, Vol. 452-453, 203278. https://doi.org/10.1016/j.wear.2020.203278

[Hloch 2022] Hloch, S., et al. Subsurface microtunneling in ductile material caused by multiple droplet impingement at subsonic speeds. Wear, 2022, Vol.490-491, 204176. https://doi.org/10.1016/j.wear.2021.204176

[Hloch 2024] Hloch, S., et al. Submerged pulsating water jet erosion of ductile material. Wear, 2024, Vol.538-539, 205243. https://doi.org/10.1016/j.wear.2024.205243

[Hloch 2024 b] Hloch, S., et al. Erosion development in AISI 316L stainless steel under pulsating water jet treatment, Engineering Science and Technology, an International Journal, 2024, Vol.50, 101630. https://doi.org/10.1016/j.jestch.2024.101630

[Hong 2023] Hong, S., et al. Investigation on the erosion characteristics of liquid–solid two-phase flow in tee pipes based on cfd-dem. Journal of Marine Science and Engineering, 2023, Vol.11, No.12, 2231. https://doi.org/10.3390/jmse11122231

[Lehocka 2019] Lehocka, D., et al. Comparison of ultrasonically enhanced pulsating water jet erosion efficiency on mechanical surface treatment on the surface of aluminum alloy and stainless steel. The International Journal of Advanced Manufacturing Technology, 2019, Vol.103, pp 1647-1656. https://doi.org/10.1007/s00170-019-03680-8

[Louis 2007] Louis, H., et al. Abrasive water suspension jet technology fundamentals, application and developments. Welding in the World, 2007, Vol.51, pp 11-16. https://doi.org/10.1007/BF03266595

[Ma 2015] Ma, D., et al. Water impingement erosion of deep-rolled Ti64. Metals, 2015, Vol.5, No.3, pp 1462-1486. https://doi.org/10.3390/met5031462

[Nag 2019] Nag, A., et al. Acoustic chamber length performance analysis in ultrasonic pulsating water jet erosion of ductile material. Journal of Manufacturing Processes, 2019, Vol.47, pp 347-356. https://doi.org/10.1016/j.jmapro.2019.10.008

[Nag 2023] Nag, A., et al. Comparison of continuous and pulsating water jet during piercing of ductile material. Materials, 2023, Vol.16, No.9, 3558. https://doi.org/10.3390/ma16093558

[Nag 2024] Nag, A., et al. Maximization of wear rates through effective configuration of standoff distance and hydraulic parameters in ultrasonic pulsating waterjet. Facta Universitatis, Series: Mechanical Engineering, 2024, Vol.22, No.2, pp 165-186. https://doi.org/10.22190/FUME220523045N

[Poloprudsky 2019] Poloprudsky, J., et al. Effect of standoff distance on the erosion of various materials. International Conference on Water Jet-Research, Development, Applications. Cham: Springer International Publishing, 2019. https://doi.org/10.1007/978-3-030-53491-2_18

[Poloprudsky 2021] Poloprudsky, Jakub, et al. Identification of local microplasticity on Ti6Al4V after impingement of periodically acting water clusters. International Conference on Manufacturing Engineering and

Materials. Cham: Springer International Publishing, 2021. https://doi.org/10.1007/978-3-030-71956-2_6

[Poloprudsky 2022] Poloprudsky, J., et al. Effects of liquid droplet volume and impact frequency on the integrity of Al alloy AW2014 exposed to subsonic speeds of pulsating water jets. Wear, 2022, Vol.488-489, 204136. https://doi.org/10.1016/j.wear.2021.204136

[Poloprudsky 2024] Poloprudsky, J., et al. Water droplet erosion assessment in the initial stages on AISI 316 L using kernel average misorientation. Tribology International, 2024, Vol.191, 109165. https://doi.org/10.1016/j.triboint.2023.109165

[Siahpour 2022] Siahpour, P., et al. Surface characteristics and residual stress generation in Ti-6Al-4 V following ultrasonic pulsed water jet peening. Surface and Coatings Technology, 2022, Vol.445, 128691. https://doi.org/10.1016/j.surfcoat.2022.128691

[Siemers 2018] Siemers, C., et al. Aluminum-and vanadium-free titanium alloys for application in medical engineering. In Titanium in medical and dental applications, Woodhead Publishing, 2018, pp 477-492. https://doi.org/10.1016/B978-0-12-812456-7.00021-4

[Song 2020] Song, C., and Cui, W. Review of underwater ship hull cleaning technologies. Journal of Marine Science and Application, 2020, Vol.19, No.3, pp 415-429. https://doi.org/10.1007/s11804-020-00157-z

[Stolarik 2023] Stolarik, G., et al. Titanium surface roughening with ultrasonic pulsating water jet, Journal of Manufacturing Processes, 2023, Vol.90, pp 341-356. https://doi.org/10.1016/j.jmapro.2023.02.013

[Stolarik 2024] Stolarik, G., et al. Submerged surface texturing of AISI 304L using the pulsating water jet method. Archives of Civil and Mechanical Engineering, 2024, Vol.24, No.4, 207. https://doi.org/10.1007/s43452-024-01029-x

[Srivastava 2020] Srivastava, M., et al. Standoff distance in ultrasonic pulsating water jet. Materials, 2020, Vol.14, No.1, 88. https://doi.org/10.3390/ma14010088

[Szada-Borzyszkowska 2023] Szada-Borzyszkowska, M., et al. Analysis of the pulsating properties of a high-pressure water jet generated in a self-excited head for erosion processing. Archives of Civil and Mechanical Engineering, 2023, Vol.23, No.4, 236. https://doi.org/10.1007/s43452-023-00769-6

[Thomas 1970] Thomas, G. P., and Brunton, J. H. Drop impingement erosion of metals. Proceedings of the Royal Society of London. A. Mathematical and Physical Sciences, 1970, Vol.314, No.1519, pp 549-565. https://doi.org/10.1098/rspa.1970.0022

[Wright 2013] Wright, M. M., et al. Cavitation of a submerged jet. Experiments in fluids, 2013, Vol.54, pp 1-21. https://doi.org/10.1007/s00348-013-1541-3

[Yadav 2016] Yadav, H., et al. Characterization of pulsating submerged jet - A particle image velocimetry study. Journal of Thermal Science and Engineering Applications, 2016, Vol.8, No.1, 011014. https://doi.org/10.1115/1.4030813

[Xiaohui 2021] Xiaohui, L., et al. Research on the underwater noise radiation of high pressure water jet propulsion. Ocean Engineering, 2021, Vol.219, 108438. https://doi.org/10.1016/j.oceaneng.2020.108438

[Zelenak 2015] Zelenak, M., et al. Visualisation and measurement of high-speed pulsating and continuous water jets. Measurement, 2015, Vol.72, pp 1-8. https://doi.org/10.1016/j.measurement.2015.04.022

CONTACTS:

Ing. Jakub Poloprudsky, Ph.D.
Institute of Physics of Materials, The Czech Academy of Sciences
Zizkova 513/22, Brno, 616 00, Czech Republic
+420 532 290 345, poloprudsky@ipm.cz, www.ipm.cz